JOURNAL OF SPACECRAFT AND ROCKETS
Vol. 33, No. 4, July–August 1996

Measured Spacecraft Instrument and Structural Interactions

Ansel J. Butterfield*
Bionetics Corporation, Hampton, Virginia 23669
and
Stanley E. Woodard†
NASA Langley Research Center, Hampton, Virginia 23681

Evaluation of flight data from the Upper Atmosphere Research Satellite shows that the solar-disk tracking subsystem within the Halogen Occultation Experiment responds to and completely accommodates cyclic disturbances from the spacecraft solar-array vibration and continuous scanning motions by the High-Resolution Doppler Imager instrument. A fine sun sensor within the Halogen Occultation Experiment senses the top egde of the solar disk as the primary tracking control input. Data streams from such sensing show a characteristic frequency, which is principally determined by the apparent solar motion. Power-spectral-density renderings of sun sensor data streams show the disturbing frequencies as sideband peaks around a central peak at the characteristic frequency. The sidebands are analogous to frequency modulation of a carrier frequency. A mathematical model developed for this analysis demonstrates the factors that influence the frequency-modulated measurements. Modeling analyses verified the frequency content and allowed estimates of local relative amplitudes of the principal disturbances imparted to the spacecraft. The model can predict mutual interactions between instruments as well as the influence of structural excitations upon instruments. This analysis offers a means toward evaluating potentials for adverse interactions in cases where a spacecraft carries closed-loop instruments that track fixed solar or stellar targets; such interactions can become crucial if tracking requirements have small margins of error.

Nomenclature

A_c	= carrier amplitude of frequency-modulated response, arc seconds
A_1, A_2, A_3	= amplitudes of periodic disturbances, arc seconds
t	= time, s
x	= frequency-modulated response, ″
ω_c	= carrier frequency of frequency-modulated response, Hz
$\omega_1, \omega_2, \omega_3$	= frequencies of periodic disturbances, Hz

Introduction

THE advent of multipayload spacecraft with elastically flexible appendages requires spacecraft designers to have knowledge of any mutual interactions between payloads as well as any control–structure interactions.[1–5] Multipayload spacecraft offer both temporal and spatial coregistration of in-flight observations; spacecraft design must meet jitter requirements at the boresight of each science instrument to allow accurate coregistration. Jitter is the measure of spacecraft attitude change during a reference time interval. This paper presents observations and related analyses of disturbance effects from the Upper Atmosphere Research Satellite (UARS) solar-array vibration and the High-Resolution Doppler Imager (HRDI) on the Halogen Occultation Experiment (HALOE) instrument. UARS in the on-orbit deployed configuration is shown in Fig. 1, which also identifies the features and science instruments pertinent to this study. An overview of the UARS is presented. HRDI and HALOE are overviewed to show how each contributes to the overall dynamic response of the platform, and to describe their control logic. Then observations and analysis of the influence of one science payload on the other are presented. These observations were used to develop a mathematical model to describe how one payload can influence another and what factors are critical in such interactions.

Received Feb. 28, 1995; revision received July 26, 1995; accepted for publication Aug. 28, 1995.

*Project Engineer, Suite 1000, 2 Eaton Street.
†Aerospace Engineer, Structural Dynamics Branch, Structures Division, MS 230. Member AIAA.

Overview of the UARS Spacecraft

The UARS observatory (Fig. 1) includes 10 science instruments mounted on an instrument module (IM), which is affixed to a multimission modular spacecraft (MMS) that provides attitude control, communication, data handling, electrical power distribution, and propulsion. The IM also carries a high-gain antenna for communication links, a solar stellar pointing platform that carries three of the instruments, and a solar array consisting of six panels. In addition to the suite of science instruments, UARS has two elastically flexible appendages that can be excited by disturbance sources onboard the spacecraft. Onboard disturbances are caused by UARS's five gimballed instruments and subsystems, the solar array, MMS reaction wheels, the propulsion subsystem, and thermal snap of the solar array as the spacecraft passes through the Earth's terminator. These disturbances can affect the precision pointing of the remote sensing instruments and coregistration of measurements. Disturbances imparted to the platform during the course of an orbit can occur as impulses, ramped forces, or periodic excitations. Continuous periodic excitations result from HRDI and the Microwave Limb Sounder instruments that determine altitude profiles of atmospheric

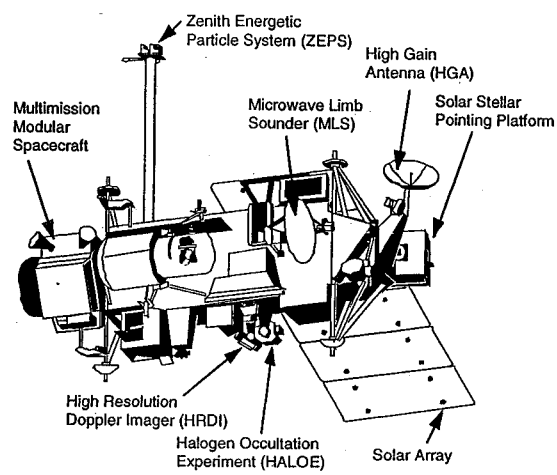

Fig. 1 Features and science instruments of the UARS.

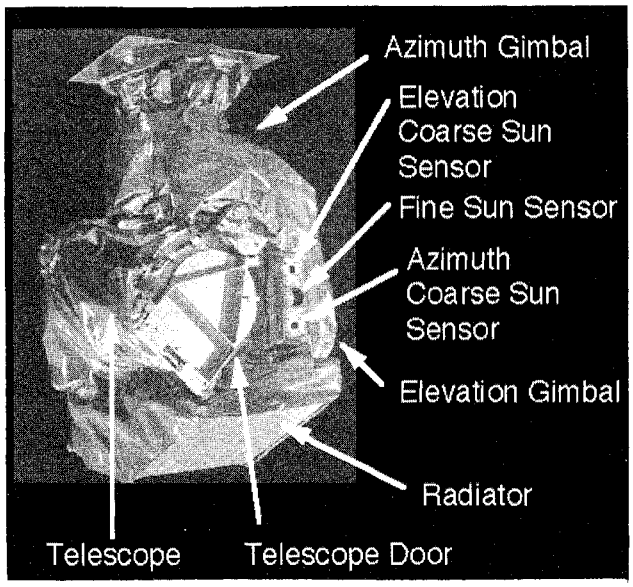

Fig. 2 Features of the halogen occultation experiment.

parameters by making vertical scans or a combination of both horizontal and vertical scans. As a spacecraft, the UARS accommodated all imposed disturbances and maintained a controlled attitude within the 108″ specification limit for all three axes.[5]

The UARS attitude control system has a number of onboard sensors for attitude determination; however, only the rate gyros in the inertial reference unit (IRU) could determine attitude to the precision needed for a jitter study. These gyros have a resolution of 0.05″ (one telemetry count) and a sampling rate of 7.8125 Hz. The IRU is at one end of the spacecraft, and it was desired to know if motions were the same throughout the spacecraft. The HALOE science instrument, shown in Fig. 2, offered a means for such a determination. HALOE carries a coarse sun sensor (CSS) with a resolution of 2.0″ sampled every 0.128 s, and a fine sun sensor (FSS) with a resolution of 16.2″ sampled every 0.016 s. HALOE determines the vertical distribution of several atmospheric species while viewing the sun through the Earth's atmosphere during orbital sunrise and sunset events. Once the HALOE gimbal positions have acquired the solar disk, FSS measurements are used to control the elevation attitude of a two-axis gimbal assembly, which tracks the sun and positions the telescope boresight on the solar disk in a manner to satisfy the science instrumentation. This precise pointing system accommodated spacecraft orbital motion combined with jitter disturbances, and thereby offered a means to determine local jitter motions.

HRDI Overview

The HRDI instrument is mounted amidship on UARS (Fig. 1). HDRI observes the Doppler shifts of spectral lines within the atmospheric band system of molecular oxygen. A triple-etalon Fabry–Perot interferometer serves as a high-resolution spectral filter to reject continuum emissions outside the desired absorption lines. The interferometer is mounted within a two-axis gimbaled telescope, whose motion is controlled by a microprocessor. The HRDI sequence first measures Doppler shifts while performing a vertical altitude scan in the direction forward of the spacecraft's velocity. The telescope is then rotated 90 deg, and a second vertical altitude scan is performed. This scan sequence yields two measurements over the same region of the atmosphere in a time interval that is short (less than 7 min) compared to the characteristic time scales for changes in the wind field. These measurements, coupled with knowledge of spacecraft velocity and observation geometry, allow calculations of horizontal vector wind fields extending from the upper troposphere through the thermosphere. HRDI measurement requirements impose a 36″ limit on spacecraft platform jitter motion over any 0.128-s time interval.[5] HRDI has one continuous, periodic open-loop scan profile for the day and a second, shorter-period open-loop scan profile for the night portion of the orbit.

HALOE Overview

The HALOE instrument, shown in Fig. 2,[6,7] is also mounted amidship on UARS near the HRDI instrument. This experiment measures the vertical distribution of O_3, HCl, HF, NO, CH_4, H_2O, and NO_2 over the altitude range from 10 to 65 km (tangent height) with a vertical resolution of 2 km. It also measures the atmospheric pressure. As the sun–spacecraft line of sight transverses the Earth's limb during orbital sunrise and sunset events, chemical species in the atmosphere absorb infrared energy in well-defined wavelength bands, which are then measured by HALOE. Because the sun is used as a constant light source, instrument pointing must be kept within a specific area on the solar disk that only extends 120″ in elevation by 360″ in azimuth. A stepper-motor-driven biaxial gimbal system, the CSS, the FSS, and a microprocessor-based closed-loop feedback tracking control logic provide the pointing accuracy. The independently controlled gimbals have a ±185-deg azimuth range and a 39-deg elevation range. Both the CSS and the FSS provide error signals to the control algorithm.

HALOE autonomously performs solar acquisition, solar scan, calibration, track, and stow sequences. Operations alternate between sunrise and sunset sequences. Sunset sequences begin with a solar coarse acquisition into fine track, the fine track itself, a programmed time delay, an instrument balance procedure, five solar scan cycles, a calibration sequence, a science data retrieval period, and a slew to stow for the night stow location. The sunrise sequence is the same as the sunset reversed, except that the time delay and balance modes do not occur and a boresight check occurs immediately prior to the day stow position.

The elevation axis uses an analog CSS for initial solar acquisition. Once the sun has been acquired, the FSS provides for solar scanning and tracking; Fig. 3 shows a schematic of the FSS. The array contains 256 silicon photodiode elements installed to provide an angular spacing of 16.2″. In the absence of atmospheric distortions, the solar image covers 118 elements. The telescope axis is boresighted to photodiode element 140. During fine tracking operation, one particular diode is selected as the reference for positioning the top edge of the solar disk. Diode 108 was the reference for the measurements described in this paper. The FSS output data are diode numbers that show the position of the top sun edge (TSE) sampled every 0.016 s and the bottom sun edge sampled every 0.128 s. The TSE provides the error input for the control law for both scanning and tracking modes. In the track mode, the reference TSE is subtracted from the measured TSE. This difference becomes the error signal into the control-law algorithm, which in turn commands zero, two, or four elevation steps from the stepper motor in the direction for minimizing the track error. Stepper-motor gearing provides motion in increments of 16.2″ to match the diode angular spacings. The control law updates at 0.128-s intervals to keep the maximum misalignment and corresponding track error within one step (16.2″) after the execution of gimbal motion commands.

During elevation fine track operations, the apparent solar motion equates to the spacecraft orbit angular rate multiplied by the cosine of the solar angle (angle between the orbit plane and direction to the sun). HALOE data sequences involve apparent solar motions

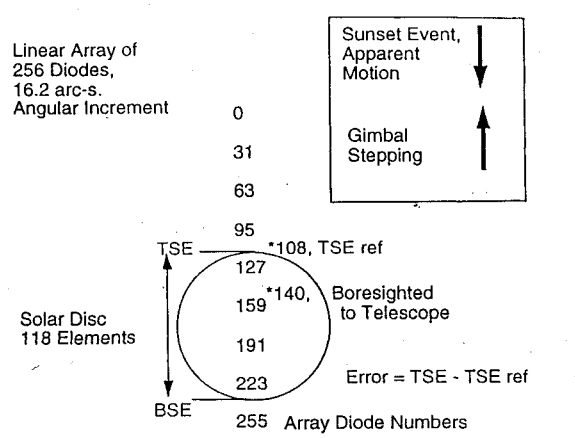

Fig. 3 Features of the HALOE FSS diode array.

Table 1 Error signal and commanded gimbal steps

Measured error, TSE−(TSE ref)	Commanded gimbal steps
0	0
1	0
2	2
3	4
4	4

Table 2 HALOE control-law operation and telemetry responses for an angular motion of 22″ during a control interval of 0.128 s

Control Interval	Angular offset, arc seconds	FSS illuminated diode away from TSE ref.[a] 1 2 3 4 5 6 7 8	Commanded gimbal steps
0	0	0	
1	+22	0 0 0 1 1 1 1 1	0
2	+44	1 2 2 2 2 2 3 3	4
3	+66−64.8 = 1.2	3 3 3 3 4 4 4 0	0
4	+23.2	0 0 1 1 1 1 1 1	0
5	+45.2	2 2 2 2 2 3 3 3	4
6	+67.2−64.8 = 2.4	3 3 3 4 4 4 4 0	0
7	+24.4	0 0 1 1 1 1 1 2	2
8	+46.4−32.4 = 14	2 2 2 2 3 3 3 1	0
9	+36	1 1 1 1 2 2 2 2	2
10	+58−32.4 = 25.6	2 3 3 3 3 3 3 2	2

[a]FSS sample number between gimbal updates.

that range from about 16 to 30″ over each 0.128-s control interval. Gimbal motions occur at time intervals that are increments of 0.128 s, which corresponds to an excitation frequency of 7.815 Hz. A disturbance at this frequency is well above the 0.01-Hz bandwidth for the UARS attitude control system and enters the spacecraft unimpeded. While UARS appeared insensitive to this frequency, such a frequency could become a concern in other applications that required closer tracking tolerances.

An example of HALOE control-law operation begins with the HALOE elevation gimbal error signal as the difference between the measured TSE and the desired or baseline diode, TSE ref. The number of commanded gimbal steps is dependent upon the measured error. Typical cases for the error and number of commanded gimbal steps are shown in Table 1. The FSS data stream for analysis consists of the diode numbers corresponding to the top edge of the sun. A histogram is generated by the combination of apparent solar motion illuminating diodes sequentially in one direction for eight measurements at 0.016-s intervals, countered by gimbal stepping in the opposite direction at 0.128-s intervals. Table 2 illustrates how such a control law would operate for the case of 22″ of apparent solar motion over a control interval of 0.128 s. The table shows the angular offset at the end of each control interval, the pattern of diode illumination data, the diode that would generate the error signal (the eighth FSS sample provides the error input that is executed between the seventh and eighth samples in the next control interval), and the gimbal motion that would result from the control logic. The gimbal steps generate repetitive patterns with repetition sequences that appear characteristic of an orbit event. For the example, a complete repetition sequence shown in Table 2 covers about 40 control intervals, and also shows that only a four-step gimbal correction reilluminates the reference diode.

Observations Using In-Flight Telemetry

Opportunities for observation and analysis of flight data from orbital sunset events occurred on Jan. 28, 1992 (day 139 after launch), and on May 1, 1992 (day 233 after launch). Operations on day 139 were at a solar angle of 38 deg with the UARS in a forward flight mode (MMS to the rear, Fig. 1) and all instruments in normal operation (HRDI in night scan). Operations on day 233 were at a solar angle of 2 deg with UARS in a backwards flight mode (MMS leading; Fig. 1; solar array rotates in the opposite direction). Flight data covered two sequential sunset events: the first with all instruments in normal operation, the second with only HALOE in operation (HRDI stationary).

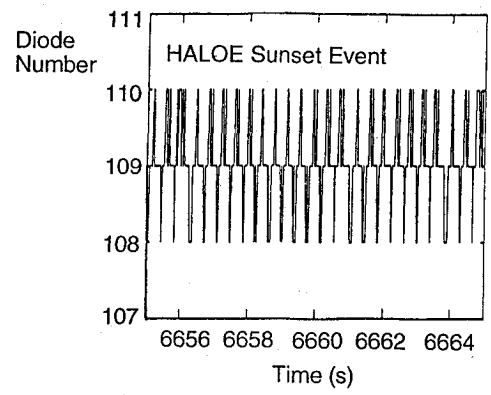

Fig. 4 HALOE FSS illuminated diodes for 10 s of day 139. 1 Diode = 16.2″.

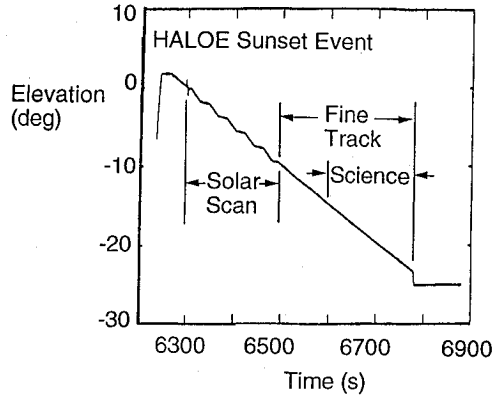

Fig. 5 HALOE elevation gimbal angle, day 139.

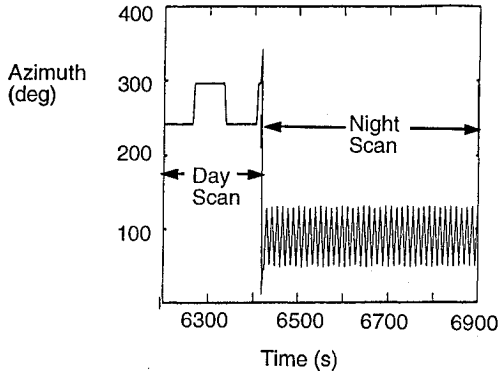

Fig. 6 HRDI azimuth gimbal position, day 139.

The time history for FSS illumination during 10 s from day 139 is shown in Fig. 4. Diode 108 is the reference diode that the control logic will always try to reilluminate. This histogram consists of diode numbers sampled every 0.016 s, with number changes away from 108 because of apparent solar motion, and number changes toward 108 to gimbal stepping at increments of 0.128 s. Diode 108 was reilluminated about 24 times during this 10-s data interval and, from the example outlined in Table 2, required a four-step correction (gimbal motion was 64.8″ during the course of a 0.128-s control interval). The elevation gimbal-angle time history is shown in Fig. 5 with two operating modes of the instrument annotated. In the solar scan mode, HALOE scans the disk of the sun up and down five times; in the fine track mode, HALOE makes its science measurements. During HALOE science measurements, HRDI is operating with its night scan as shown in Fig. 6. This night-scan frequency of 0.083 Hz is also outside the 0.01-Hz bandwidth of the UARS attitude control system and therefore enters the spacecraft structure unimpeded. The UARS yaw angular-position history for the same orbit time interval is shown in Fig. 7, and reveals that HRDI scanning results in about 4″ in cyclic yaw motion of the spacecraft. The anomaly toward the end

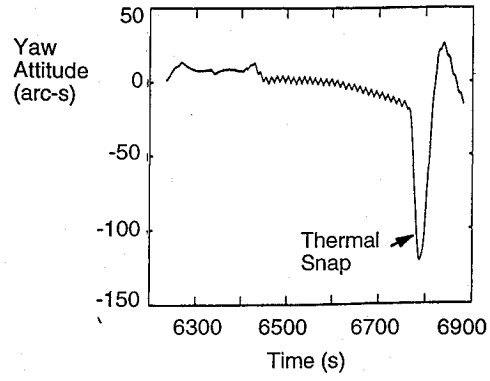

Fig. 7 Spacecraft yaw attitude, day 139.

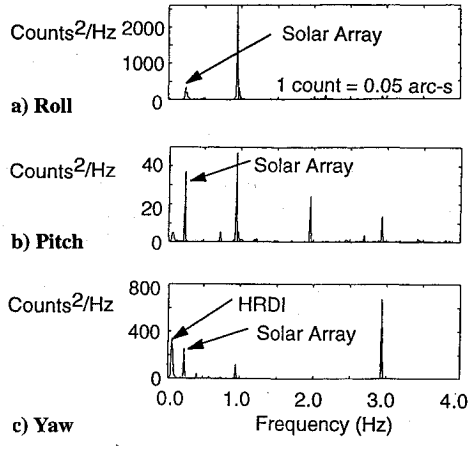

Fig. 8 PSD for UARS rate-gyro telemetry data, day 139.

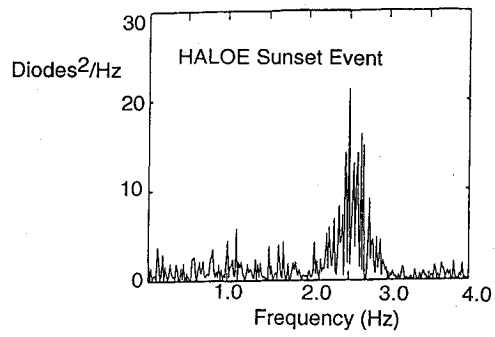

Fig. 9 PSD for HALOE FSS telemetry data, day 139. 1 Diode = 16.2″.

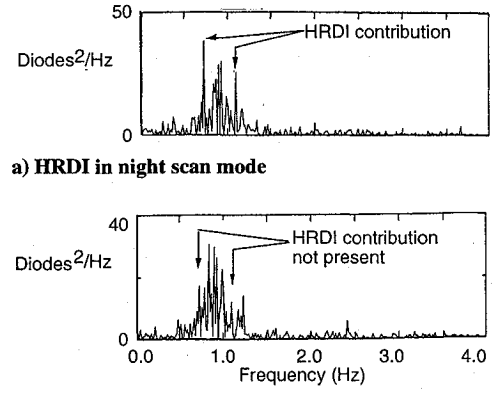

Fig. 10 PSD for HALOE FSS telemetry data, day 233. 1 Diode = 16.2″.

of the yaw-position time history is the result of solar-array thermal snap caused by thermal gradients in the solar array each time the spacecraft transits the Earth's terminator.

The HRDI night-scan frequency (0.083 Hz) combines with a solar-panel vibration frequency at approximately 0.25 Hz. The effects can be observed in power spectral density (PSD) renderings from gyro response measurements; Figs. 8a, 8b, and 8c show such PSD for roll, pitch, and yaw gyro time histories. Solar-array vibration appears at about 0.25 Hz in all three axes; HRDI disturbances appear at 0.083 Hz in the pitch and yaw axes. The yaw-axis response stems from the fore–aft scanning; a much smaller pitch response reflects the four-step elevation scan and return included in the total HRDI motion. Higher-frequency responses at about 1, 2, and 3 Hz are attributed to bending-mode excitations of the boom that supports the Zenith Energenic-Particle System (ZEPS; Fig. 1). All can influence the HALOE line-of-sight pointing; however, only the solar array and HRDI cause motions of a magnitude that can be observed using the HALOE FSS. HRDI scanning and solar-array vibration influence HALOE fine tracking in a manner that appears as frequency modulations to the wave shape generated by the FSS histogram.

The frequency content of the FSS diode readings (Fig. 4) is shown as a PSD rendering in Fig. 9. A dominant frequency appears at 2.497 Hz with several frequencies banded around it. For reference, all PSDs were produced by an algorithm that accepts up to 8192 data samples. It truncates input time histories so that it retains the maximum number of samples that can be expressed by integer powers of 2. Time histories were 65 s and provide up to 4096 data samples—the maximum compatible with HALOE fine track operating times. Rectangular windows were used. A PSD is produced by multiplying the fast Fourier transform of the truncated time history with its complex conjugate and then normalizing the product by the number of samples used.

The 2.497-Hz dominant frequency in Fig. 9 corresponds to the rate of FSS reference diode reillumination by the combination of apparent solar motion and control-law stepping of the elevation gimbal. (Fig. 4 shows 24 times in 10 s.) At the same orbital times, the frequency content for the spacecraft roll, pitch, and yaw motions as shown by Figs. 8a, 8b, and 8c are considered indicative of the frequency content for the motion at the base of HALOE, since the primary structure to which the IRU and HALOE are affixed is quite rigid. Thus, over the same orbital time period (6655–6760 s past the start of day 139) the PSDs for all three gyros show that a frequency is present near 0.25 Hz due to the solar-array vibration; in addition, the yaw and pitch gyros show a frequency near 0.083 Hz, the frequency of the HRDI azimuth gimbal during the night scan. There appears to be no direct correlation between FSS and gyro PSD renderings.

Because HALOE gimbal motions are determined by an error signal produced at 0.128-s intervals, small spacecraft jitter motions are sensed in combination with a much greater apparent solar motion. The elevation gimbal must step from 10 to 15 of its 16.2″ increments to follow the sun over one second of orbit time. Accommodation of apparent solar motion alone results in a repetitive pattern of two- and four-step changes (Table 2), and the frequency of four-step changes dominates in a PSD rendering. When other disturbances (i.e., due to instruments and subsystems) are present, HALOE's control logic will reposition its elevation gimbal to remove the related pointing jitter for vibrations up to about 10 Hz. This will produce a pattern of zero, two, and four angular step changes, which will not necessarily be repetitive. The effect of the HRDI instrument and the solar-array vibration is to perturb the nominal stepping of the elevation gimbal motion. Disturbances in angular position will appear as cyclic additions to or subtractions from the apparent solar motion. In a PSD rendering of FSS data, this interaction of HRDI and the solar array on HALOE produces a measurable magnitude and frequency correlation within the bands of spectra around the dominant frequency of the reference-diode reillumination.

A confirmation of such interactions can be shown by comparing flight data from day 139 with flight data from day 233. PSD renderings of FSS data for successive orbit sunset events on day 233 appear in Figs. 10a and 10b for comparison with Fig. 9. Operation on day 139 was at a solar angle of 38 deg, and an apparent solar motion of 173″/s was accommodated with a stepping motion that reilluminated

the reference diode at about 2.5 Hz. Most of the gimbal motions involved four-step (64.8″) corrections. Operation on day 233 was at a solar angle of 2 deg, and an apparent solar motion of 226″/s was accommodated with gimbal stepping that reilluminated the reference diode at frequencies of 0.8 and 1.0 Hz. Fine track accommodation involved a sequence that made one four-step correction (64.8″) followed by about five two-step corrections (32.4″ each). The reference diode reillumination frequency appears at about 1 Hz, which correlates to a four-step correction and also appears as a center for banding. (The smaller corrections at lower amplitude appear at a frequency above 4 Hz and are not shown.) Thus, the frequencies about which the bands are centered are the frequencies at which the reference diode is reilluminated and correlate to 64.8″ corrections. All three renderings show the characteristic banding associated with disturbing jitter frequencies; however, there is a significant difference between the banding patterns in Figs. 10a and 10b. These traces represent successive orbits. The difference is in the operation of the HRDI instrument, as shown in Fig. 10a for operation with HRDI in its night-scan mode generating a jitter frequency at 0.083 Hz and in Fig. 10b for operation during the next orbit with HRDI stationary. The difference between the two traces (i.e., the absence of the two annotated sidebands) represent the HRDI contribution at 0.083 Hz to the local jitter environment. These sidebands appear as frequency peaks 0.083 Hz away from the frequencies associated with reillumination of the reference diode and four-step gimbal corrections. During the solar event that resulted in the PSD of the FSS diode time history represented in Fig. 10a, diode reillumination occurred at both 0.8 and 1.02 Hz. The peak at 0.720 Hz corresponds to a first lower modulation sideband 0.083 Hz below 0.8 Hz. The peak at 1.076 Hz corresponds to a first higher-modulation sideband 0.083 Hz above 1.02 Hz. These combinations are within the PSD spectral resolution limits of ±0.01525 Hz.

Payload–Payload Interactions and Structure–Payload Interactions

Interactions occur aboard the UARS, and Fig. 11 shows how the spacecraft platform serves as a conduit for such disturbances. Disturbances excite the flexible appendages, which vibrate and result in spacecraft jitter. The jitter, in turn, affects the line of sight of the fixed-mounted and open-loop science instruments and subsystems. Closed-loop tracking systems must accommodate the jitter to maintain their line-of-sight pointing. In the process of maintaining their line-of-sight pointing, they impart disturbances to the spacecraft, whose frequencies and amplitudes are dependent on the resulting inputs to their control logic; Ref. 5 presents a comprehensive assessment and technique for analysis of such interactions.

For UARS, the disturbances imparted by HRDI and the solar array are considered sinusoidal, and since they are continuously excited, they are also considered undamped and constitute a sinusoidal jitter. Each jitter response will have a specific amplitude and frequency. In application to HALOE tracking, a wave shape is formed in the FSS data stream as the apparent solar motion sequentially illuminates diodes away from the reference diode while the elevation gimbal control logic restores the illumination to the reference diode. This combination results in reillumination of the reference diode at a frequency that is dependent upon the solar angle. Frequencies due to spacecraft jitter cause periodic positive and negative shifts away from the desired reference diode. The result is the periodicity due to spacecraft motion being embedded in the periodic updating of the reference diode. A continuous-function approximation of the FSS diode illumination time history can be expressed as follows:

$$x = A_c\sin[2\pi\omega_c t + A_1\sin(2\pi\omega_1 t) + A_2\sin(2\pi\omega_2 t)] \quad (1)$$

Equation (1) is similar to that for frequency modulation used in radio transmissions. For this case, all amplitudes in the function are expressed in arc seconds. The carrier amplitude, using the FSS, occurs in increments of 16.2″ and is defined by the maximum number of diodes illuminated in 0.128 s or the number of gimbal steps required to reilluminate the reference diode. The carrier frequency is the rate of reillumination for the reference diode. The amplitudes of the modulating frequencies are the amplitudes for the jitter due to HRDI and the solar array, respectively, and the modulating frequencies are the frequencies of the jitter due to HRDI and the solar array, respectively. The continuous function (1) can be compared with the discrete FSS diode time history. In the frequency domain (PSD), they can be compared by observing the frequency bands about the carrier fundamental.

Jitter frequencies and amplitudes due to HRDI and solar-array disturbances can be derived by doing system identification in an unconventional manner. Analysis of data from day 139 showed the reference diode was reilluminated at a rate of 2.561 Hz by a four-step gimbal motion. This corresponds to an angular displacement of 64.8″, which can be used for the carrier amplitude in Eq. (1). Jitter frequencies due to HRDI and the solar array can be obtained from gyro PSD data (Figs. 8a–8c). PSD renderings of Eq. (1) are shown in Figs. 12 and 13 for frequencies and amplitudes as annotated. The PSDs show sideband patterns that are indicative of the modulating frequencies. These appear as the modulating frequencies added to or subtracted from the carrier frequency for some of the bands. Other bands are the sums and differences of the modulating frequencies added to or subtracted from the carrier frequency. Modulation sidebands resulting from HRDI and the solar-array vibrations appear annotated in Fig. 14, which is a repeat of Fig. 9. Other disturbances are present, but their effects on the FSS are not as significant.

Comparison of Figs. 12 and 13 shows that the magnitudes of the sidebands exhibit a strong dependence upon the modulation amplitudes. The ratio of PSD sideband magnitudes to that of the carrier frequency can be adjusted by assigning modulation amplitudes. When these ratios as derived using Eq. (1) match those obtained from FSS data analysis, then the assigned modulating amplitudes are determined as the jitter amplitudes caused by HRDI and the solar array. Utilization of the ratios of PSD sideband to center-frequency-band magnitudes allows correlation of analytic results

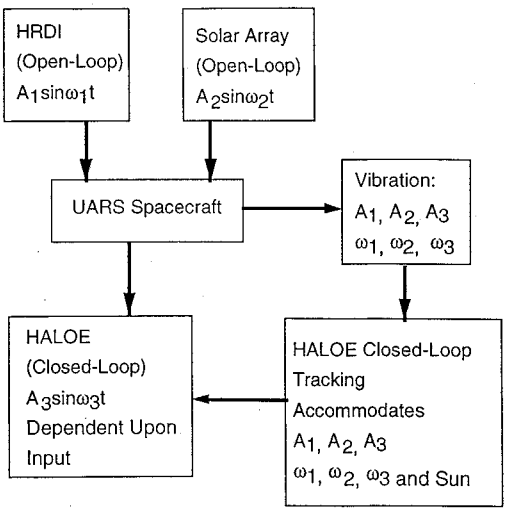

Fig. 11 Interactions of UARS onboard instruments and structures.

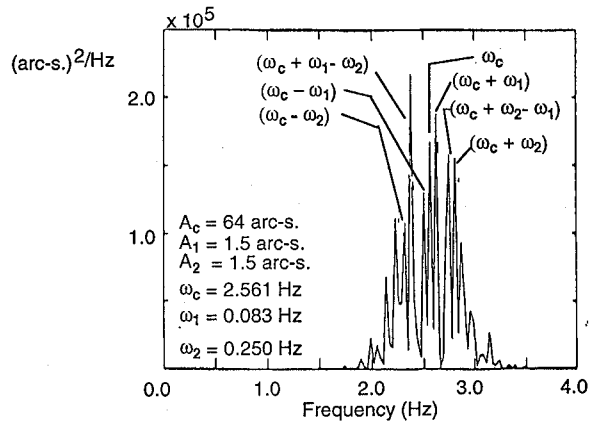

Fig. 12 PSD for a waveform generated by Eq. (1), case 1.

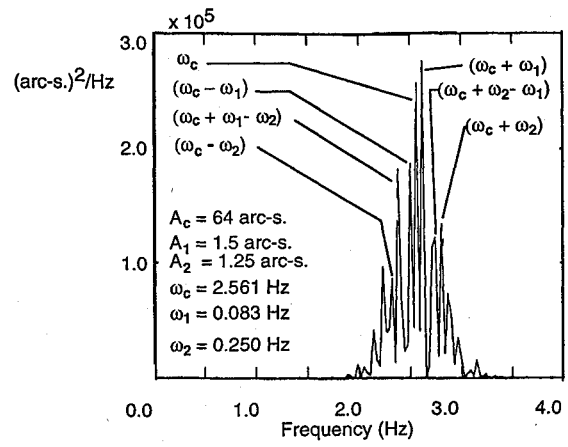

Fig. 13 PSD for a waveform generated by Eq. (1), case 2.

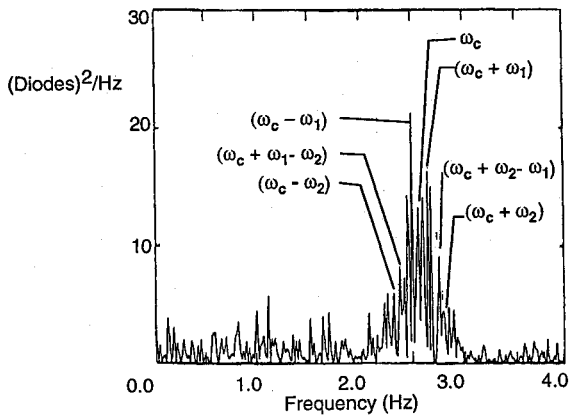

Fig. 14 PSD for HALOE FSS telemetry data for day 139 with disturbance frequencies annotated.

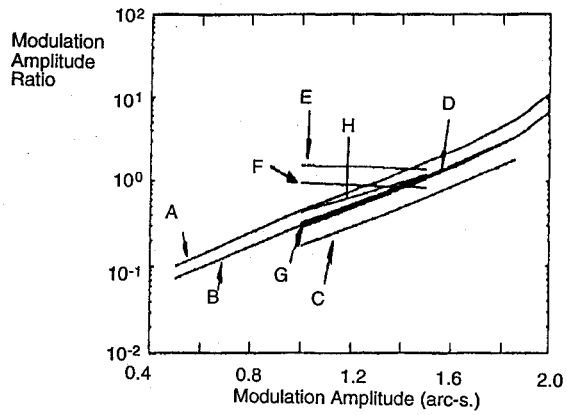

Fig. 15 Ratios of PSD-sideband to carrier-frequency-band magnitudes for jitter amplitudes.

in actual dimensions with flight data [e.g., (arc seconds)^2/Hz with (diodes)^2/Hz].

PSD renderings of Eq. (1) with only a single modulating frequency were performed over a range of modulation amplitudes for both the HRDI frequency at 0.083 Hz and the solar array at 0.25 Hz. The ratio of magnitudes for the first sidebands to the magnitude of the carrier frequency band showed a strong dependence upon the amplitude assigned to the modulating frequency. Such magnitude ratios are shown in Fig. 15 as a function of modulating amplitude for a carrier frequency of 2.561 Hz with a carrier amplitude of 64.8″ as follows: 1) trace A: HRDI only, first-lower-frequency-band ratios (2.561 − 0.083 Hz), amplitudes from 0.5 to 2.0″; 2) trace B: HRDI only, first-upper-frequency-band ratios (2.516 + 0.083 Hz), amplitudes from 0.5 to 2.0″; 3) trace C: solar array only, first-lower-frequency-band ratios (2.561 − 0.25 Hz), amplitudes from 1.0 to 1.8″; and 4) trace D: solar array only, first-upper-frequency-band ratios (2.561 + 0.25 Hz), amplitudes from 1.0 to 1.8″.

The selection of an HRDI frequency amplitude for the combined frequency evaluation used the PSD rendering of flight data in Fig. 10a, which shows HRDI-related peaks with magnitudes greater than those for the center frequency. A comparison of magnitude ratios with traces A and B of Fig. 15 indicates 1.5 to 1.6″ as the amplitude for the HRDI jitter contribution. An amplitude of 1.5″ was selected for the HRDI frequency as a basis for evaluations with two combined jitter frequencies. Accordingly the combined frequency evaluation traces of Fig. 15 represent the following combinations: 1) trace E: combined, first-lower-frequency-band ratios (2.561 − 0.083 Hz), amplitudes 0.083 Hz at 1.5″, 0.25 Hz from 1.0 to 1.5″; 2) trace F: combined, first-upper-frequency-band ratios (2.561 + 0.083 Hz), amplitudes 0.083 Hz at 1.5″, 0.25 Hz from 1.0 to 1.5″, 3) trace G: combined, second-lower-frequency-band ratios [2.561 Hz − (0.25 − 0.083 Hz)], amplitudes 0.083 Hz at 1.5″, 0.25 Hz from 1.0 to 1.5″, 2) trace F: combined, second -lower-frequency-band ratios (2.561 + 0.083 Hz), amplitudes 0.083 Hz at 1.5″ 0.25 Hz from 1.0 to 1.5″; 3) and 4) trace H: combined, second-upper-frequency-band ratios [2.561 Hz + (0.25 − 0.083 Hz)], amplitudes 0.083 Hz at 1.5″, 0.25 Hz from 1.0 to 1.5″.

A review of the combined frequency modeling showed that the first-sideband ratios (due to HRDI), traces E and F, are relatively insensitive to variations of the second modulating frequency, and also within measurement tolerance estimates of the values obtained from single-frequency modeling (traces A and B at the 1.5″ point). Estimates of relative amplitudes then utilized the single-first-modulation-band ratios to predict the 0.083-Hz responses within flight data. The 0.25-Hz contributions were obtained by comparisons of second-band ratios in flight data with second-band ratios from the combined frequency model (traces G and H). Comparison of such ratios for day 139 flight data indicates a 0.083-Hz jitter component ranging from 1.4 to 1.6″ together with a 0.25-Hz jitter component ranging from 1.2 to 1.4″. Roll gyro data for the same time period in day 139 (telemetry-count data input to PSD; Fig. 8a) show a varying-amplitude spacecraft response at 0.25 Hz that ranged up to about 3″. Roll motion coupling into HALOE pitch motion in elevation occurs in proportion to the sine of the solar angle, 38 deg. The maximum roll disturbance would total 3 × 0.6156″ = 1.847″ of jitter at 0.25 Hz. In summary, the 1.4 to 1.6″ jitter response at 0.083 Hz was not anticipated; for 0.25 Hz, the 1.2 to 1.4″ of jitter correlates to the 1.85″ maximum predicted from roll-gyro data. The UARS structure appears to act as a rigid body in responding to excitations from HRDI and the solar array.

Results and Conclusions

An evaluation of HALOE and UARS flight data indicates that HALOE is responsive to interactions from the solar-array vibration and HRDI scanning. This study has identified and analyzed a form of disturbance interactions with an instrument pointing system. In this case the disturbing frequencies appeared as modulations embedded in the sunsensor measurements. The analysis made an application of PSD renderings for flight data in conjunction with PSD renderings of modeling data for multifrequency modulation of a carrier wave to determine the jitter content. The interactions analyzed showed that the particular pointing system accommodated the disturbances to levels within design tolerances. HALOE tracking appears as a particular case for a feedback control accommodating a deadband. In this case, response to continuous apparent solar motion resulted in a characteristic tracking frequency, and external cyclic disturbances modulated that frequency. In other similar cases, appropriate modeling, together with PSD renderings as utilized herein, may offer a means for identifying disturbance frequencies and estimating their amplitudes. Design of future spacecraft will have to consider interactions with onboard pointing systems as they provide concurrent measurements (all instruments coregister observations) and concurrent onboard autonomous control. (Does one pointing system confuse another?) These conditions become more critical and sensitive as pointing tolerances decrease.

This effort has also generated a mathematical model that will allow prediction of such disturbances. Predictions address instrument-

or payload-to-spacecraft interactions (jitter) and extend to interactions between one payload and another through the spacecraft structure. The latter can become critical when a spacecraft hosts more than one independently pointed element that has to operate with close tracking tolerances.

Acknowledgments

The authors would like to thank the following people for their assistance and support. From the NASA Langley Research Center: William L. Grantham and Jerry Newsom (Controls–Structures Interactions Office); Alvah S. Moore Jr., System Engineering Division; John G. Wells Jr., Sudha M. Natarajan, Janet L. Barnes, Michael S. Cisewski, and Stanley J. Shultz, HALOE Flight Operations Team. From the Locheed Martin Astrospace Division: Richard Quinn, Anthony Camello, Eric Tate, Mike Garnek, John Molnar, Bob Hughes, and George Futchko.

References

[1]Grantham, W. L., "NASA Future Mission Needs and Benefits of Controls–Structures Interaction Technology," NASA TM 104034, Jan. 1991.

[2]Trevathan, C. E., and Burr, P. T., "Mission Requirements Document for the Upper Atmosphere Research Satellite," NASA Goddard Space Flight Center, Document 430-1601-001, Greenbelt, MD, Sept. 1984.

[3]Molnar, J., and Garnek, M., "UARS In-Flight Jitter Study for EOS," NASA CR 191419, Jan. 1993.

[4]Butterfield, A. J., and Woodard, S. E., "Payload–Payload Interaction and Structure–Payload Interaction Observed on the Upper Atmosphere Research Satellite," American Astronomical Society, Paper 93-551, Aug. 1993.

[5]Woodard, S. E., "Analysis of Disturbances on the Upper Atmosphere Research Satellite," NASA TP L 17473.

[6]Keafer, L. S., Sullivan, E. M., Spiers, R. B., Moore, A. S., Stump, C. W., Hardesty, C. A., Beswick, A. G., Baker, R. L., Smith, D. M., and Costulis, J. A., "Halogen Occultation Experiment Instrument Description Document," HALOE-02-028C, NASA Langley Research Center, Oct. 1988.

[7]Mauldin, L. E., Moore, A. S., Stump, C. W., and Mayo, L. S., "Digital Solar Edge Tracker for the Halogen Occultation Experiment," *Optical Engineering*, Vol. 26, No. 6, 1987, pp. 513–519.

E. A. Thornton
Associate Editor